Precise measurement of near-barrier ^{8}He + ^{208}Pb elastic scattering: Comparison with ^{6}He

G. Marquínez-Durán,[1,*] I. Martel,[1] A. M. Sánchez-Benítez,[1] L. Acosta,[2] R. Berjillos,[1] J. Dueñas,[1] K. Rusek,[3] N. Keeley,[4] M. A. G. Álvarez,[5,6] M. J. G. Borge,[7] A. Chbihi,[8] C. Cruz,[7] M. Cubero,[7] J. P. Fernández-García,[6] B. Fernández-Martínez,[5] J. L. Flores,[9] J. Gómez-Camacho,[5,6] K. W. Kemper,[10] J. A. Labrador,[5] M. Marqués,[11] A. M. Moro,[6] M. Mazzocco,[12] A. Pakou,[13] V. V. Parkar,[1] N. Patronis,[13] V. Pesudo,[7] D. Pierroutsakou,[14] R. Raabe,[15] R. Silvestri,[14] N. Soic,[16] Ł. Standyło,[4] I. Strojek,[4] O. Tengblad,[7] R. Wolski,[17,18] and Z. Abou-Haidar[5]

[1]*Departamento de Ciencias Integradas, Facultad de Ciencias Experimentales, Campus de El Carmen, Universidad de Huelva, 21071 Huelva, Spain*

[2]*Instituto de Física, Universidad Nacional Autónoma de México, A.P. 20-364, Distrito Federal 01000, Mexico*

[3]*Heavy Ion Laboratory, University of Warsaw, Warsaw, Poland*

[4]*National Centre for Nuclear Research, ul. A. Sołtana 7, 05-400 Otwock, Poland*

[5]*Centro Nacional de Aceleradores (U. Sevilla, J. Andalucía, CSIC), 41092 Sevilla, Spain*

[6]*Departamento de Física Atómica, Molecular y Nuclear, Universidad de Sevilla, 41080 Seville, Spain*

[7]*Instituto de Estructura de la Materia, CSIC, 28006 Madrid, Spain*

[8]*GANIL, CEA and IN2P3-CNRS, B.P. 5027, 14076 Caen Cedex, France*

[9]*Departamento de Ingeniería Eléctrica, Universidad de Huelva, 21071 Huelva, Spain*

[10]*Department of Physics, Florida State University, Tallahassee, Florida 32306, USA*

[11]*Laboratoire de Physique Corpusculaire, 14050 Caen Cedex, France*

[12]*Dipartimento di Fisica and INFN, Universita di Padova, 35131 Padova, Italy*

[13]*Department of Physics and HINP, University of Ioannina, 45110 Ioannina, Greece*

[14]*INFN - Sezione di Napoli, Via Cintia, 80126 Napoli, Italy*

[15]*K.U. Leuven, Instituut voor Kern- en Stralingsfysica, 3001 Leuven, Belgium*

[16]*Rudjer Boskovic Institute, Bijenicka 54, 10000 Zagreb, Croatia*

[17]*Institute of Nuclear Physics PAN, Kraków, Poland*

[18]*Flerov Laboratory of Nuclear Reactions, JINR, Dubna 141980, Russia*

(Received 24 July 2016; published 29 December 2016)

Dramatic differences in the elastic scattering of the neutron rich nuclei ^{6}He and ^{8}He are found when new high quality data for the ^{8}He + ^{208}Pb system are compared with previously published ^{6}He + ^{208}Pb data at the same laboratory frame incident energy. The new ^{8}He data are of the same level of detail as for stable beams. When comparing them with those previously obtained for ^{6}He + ^{208}Pb at the same energy, it is possible to determine from the data alone that ^{6}He has a much longer range absorption than ^{8}He. However, both nuclei show significant absorption beyond their strong absorption radii. While it has been known for a long time that elastic scattering at energies around the barrier only determines the optical potential over a small distance in radial space, typically ±0.5 fm or so, both the ^{6}He and the ^{8}He imaginary potentials obtained from various optical model fits to these data are the same over a much wider range of ±1.5 fm.

DOI: 10.1103/PhysRevC.94.064618

I. INTRODUCTION

Under the right conditions precise measurements of elastic scattering angular distributions are sensitive to the details of the internal structure and associated reactions of the interacting nuclei; see, e.g., the review in Ref. [1]. It has been shown in numerous stable beam cases that the internal structure has greatest influence on the elastic scattering for heavy targets at incident energies close to the Coulomb barrier. It is now possible to measure the near-barrier elastic scattering of selected radioactive beams with the precision required for such studies, equal to the best measurements with stable beams. We present precise data for the elastic scattering of ^{8}He from a ^{208}Pb target at a laboratory frame incident energy of 22 MeV, made possible by the delivered high quality ^{8}He beam and a detector system that gave excellent mass and angle resolution over a wide angular range. This is a particularly interesting case since ^{8}He is the most neutron-rich particle-stable nucleus known, with $N/Z = 3$, and it may be compared with existing ^{6}He + ^{208}Pb elastic scattering data at the same laboratory frame incident energy [2,3]. It is an important comparison since the r.m.s. matter radii of ^{6}He and ^{8}He are identical [4], eliminating any influences on the elastic scattering simply due to differences in the size of the projectile.

There are significant differences in the properties of ^{6}He and ^{8}He that should influence the elastic scattering angular distributions. Both the S_{2n} and S_n neutron emission thresholds are lower in ^{6}He, 0.973 and 1.771 MeV, respectively, compared to 2.140 and 2.574 MeV in ^{8}He. This implies a reduced importance of breakup in systems involving ^{8}He; plus, since ^{8}He is considered to have a neutron skin rather than the neutron halo of ^{6}He, the dipole coupling to the continuum should also be weaker in ^{8}He, further reducing the influence

*gloria.marquinez@dfa.uhu.es

of breakup compared to ^{6}He. The neutron emission thresholds also impact the neutron stripping Q values; Q values for $1n$ and $2n$ stripping are $+2.07$ and $+8.15$ MeV, respectively, for ^{6}He incident on a ^{208}Pb target and $+1.35$ and $+6.98$ MeV for ^{8}He. Both these reactions are therefore better Q-matched for ^{8}He. Spectroscopic factors for the $\langle ^{6}\mathrm{He}\,|^{5}\mathrm{He}+n\rangle$ and $\langle ^{8}\mathrm{He}|^{7}\mathrm{He}+n\rangle$ overlaps are about 1.6 and 2.9 [5], respectively and those for the $\langle ^{6}\mathrm{He}|^{4}\mathrm{He}+2n\rangle$ and $\langle ^{8}\mathrm{He}|^{6}\mathrm{He}+2n\rangle$ overlaps are both about 1.0 [5]. Therefore, neutron stripping should be more important for ^{8}He; significant coupling effects due to $1n$ stripping in particular should be apparent in the elastic scattering at near-barrier energies. Preliminary accounts of this work have been published elsewhere [6–9]. We present here for the first time the final data.

II. EXPERIMENTAL PROCEDURE

The measurement was performed at the SPIRAL2 facility of the GANIL laboratory, Caen, France, where high quality beams of ^{8}He are produced by fragmentation of a 75 MeV/nucleon ^{13}C primary beam on a thick graphite target, specially designed for the production of helium isotopes. The ^{8}He ions were then reaccelerated to 22 MeV by the CIME cyclotron, and transported to the experimental hall with no impurities to give 10^{5} pps beam on target with a beam spot diameter of $\sim$3.5 mm

The experimental setup was described in Ref. [6]. It consisted of a portable reaction chamber, where a silicon detector array was mounted, and a dedicated set of collimators and beam diagnostics systems. The scattered particles and reaction fragments were detected by the GLORIA (Global Reaction Array) detection system [10], consisting of six double-sided silicon strip detector (DSSSD) particle telescopes whose positions ensure the measurement with no gaps of a continuous angular range between 15° and 165°, covering an overall solid angle of 26% of 4π. Two telescopes were located in the forward hemisphere, in the angular range between 15° and 62° in the laboratory frame (lab.), two in the backward hemisphere (117°–165° lab.), plus one above (82°–128° lab.) and one below (52°-97° lab.) the horizontal plane passing through the center of the detector array in the laboratory frame. This configuration allows for an overlap of at least 10° between contiguous telescopes. Each pixel subtended an angle of 3-4° at the target. The target, a 1.1 mg/cm^{2} thick self-supporting ^{208}Pb foil isotopically enriched to 98.43%, was rotated 60° with respect to the beam axis to avoid shadowing the detectors and allow the detection of particles around 90°.

The energy calibration of the detectors was performed using a triple alpha source (^{239}Pu, ^{241}Am, and ^{244}Cm). Throughout the experiment test signals from a low frequency (2 Hz) pulse generator module were sent to the preamplifiers to estimate the efficiency of the electronics chains and dead time.

Mass and charge identification of the reaction fragments detected by the telescopes was achieved by plotting the energy loss in the ΔE detector versus the total energy $E_{\mathrm{tot}} = \Delta E + E$, generating mass-identification spectra. Figure 1 shows a typical calibrated ΔE-E_{tot} spectrum for pixels in the lower telescope. Good separation of the different helium isotopes is achieved. However, the distinction between reaction fragments

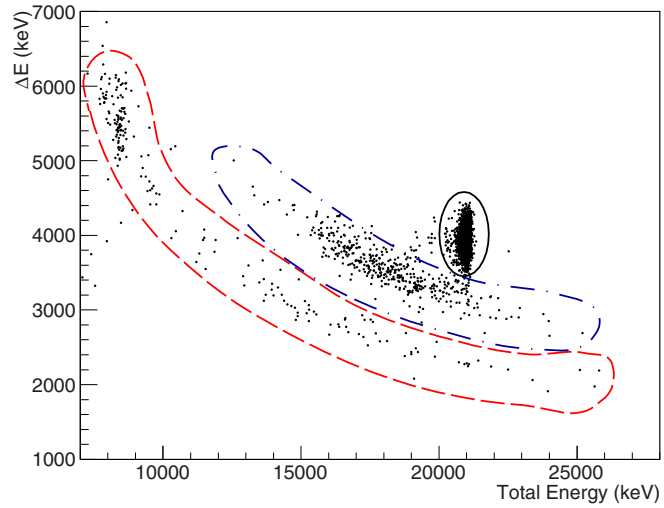

FIG. 1. Typical calibrated ΔE-E_{tot} spectrum for the lower telescope, for pixels with a laboratory scattering angle around 60° at $E_{\mathrm{lab}} = 22$ MeV. The solid ellipsoid encloses the elastically scattered ^{8}He while the dot-dashed and dashed curves enclose the ^{6}He and ^{4}He reaction fragments, respectively.

becomes difficult if the counting statistics are low. For this reason the analysis was carried out considering "summed spectra," i.e., two-dimensional spectra corresponding to the addition of single spectra from pixels with a similar scattering angle. The choice of pixels is based on the following observation: Nuclear scattering with nonpolarized ion beams generates an angular distribution with azimuthal symmetry so reaction fragments emitted with the same scattering angle are located over conical surfaces. The intersection of these surfaces with the detector plane produces a distribution of the fragments on a conic section which encloses a set of pixels with similar scattering angles, used for producing summed spectra. In Fig. 1 events corresponding to elastically scattered ^{8}He are clearly observed and separated from ^{6}He and ^{4}He produced mainly by breakup or neutron-transfer processes.

Elastic scattering data are very sensitive to a possible misalignment of the beam at the target position. Consequently, it is common practice to use stable pilot beams for the normalization of the experimental data. However, no proper pilot beam was available for this experiment and considerable effort was made to assign the scattering and solid angles of each pixel. These assignments are the result of a determination of the effective relative position of the beam spot on target with respect to the detector array (further explained in Ref. [11]). The main tool used in the search for this position was the NPTOOL package [12] for the simulation of the experimental setup, with the aim of reproducing its performance during the experiment. Once these effective positions were determined at both energies, a simulation of the whole array provided the scattering and solid angles, the angular range, and the number of events registered by each pixel considering the scattering to be pure Rutherford scattering (N_R). In this way the angular distribution of the elastic scattering differential cross section

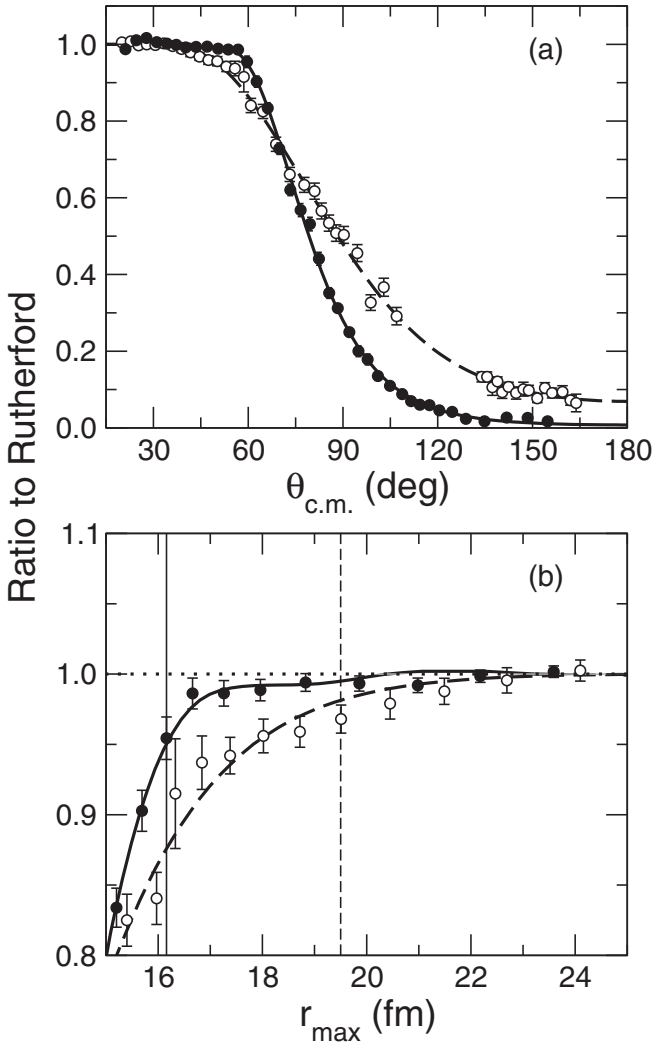

FIG. 2. (a) Angular distributions of the ^{8}He (filled circles) and ^{6}He (open circles) [2,3] + ^{208}Pb elastic scattering at 22 MeV plotted on a linear cross section scale. (b) The data plotted as a function of the classical distance of closest approach for a Coulomb trajectory, r_{max}. The solid and dashed curves denote the Woods-Saxon optical model fits of Table I to the ^{8}He and ^{6}He data, respectively. The thin solid and dashed vertical lines in (b) denote the distances at which the ^{8}He and ^{6}He +^{208}Pb elastic scattering differential cross sections first deviate from the Rutherford value by more than 2%; see text.

was obtained as follows:

$$\frac{\sigma_{\rm el}(\theta_i)}{\sigma_{\rm Ruth}(\theta_i)} = \frac{N(i)}{N_R(i)} K, \qquad (1)$$

where $N(i)$ is the number of elastic events (corrected for the efficiency of the electronics chain) detected by pixel i, $N_R(i)$ is the Rutherford yield obtained from the simulations and K is a constant determined assuming that at small scattering angles the ratio between the elastic cross section and the Rutherford cross section is 1.0. The uncertainty in the absolute angle calibration is $\pm 1.5^{\circ}$.

The resulting elastic scattering angular distribution is plotted in Fig. 2(a), together with the 22 MeV ^{6}He +^{208}Pb elastic scattering angular distribution of Refs. [2,3]. We have taken the weighted mean of adjacent points for the data of Ref. [3] for the sake of clarity. It is immediately obvious that there are important differences between the two data sets: the ^{6}He +^{208}Pb data exhibit a much less steep exponential fall-off with angle and a more marked suppression of the Coulomb rainbow peak than the ^{8}He +^{208}Pb data. In Fig. 2(b) we plot the two data sets as a function of the distance of closest approach for a classical Coulomb trajectory, r_{max}, as in Ref. [2]. The thin solid and dashed vertical lines denote the distances at which the ^{8}He and ^{6}He +^{208}Pb elastic scattering differential cross sections first deviate from the Rutherford value by more than 2%. We may consider these as the distances at which absorption begins, 16.2 fm for ^{8}He and 19.5 fm for ^{6}He, the absorption for ^{6}He having a considerably longer range than for ^{8}He. We thus see, independent of any analysis, that the elastic scattering data are sensitive to the differences in structure between ^{6}He and ^{8}He, but, as Fig. 2(b) emphasizes, precise data are required to show this.

III. OPTICAL MODEL ANALYSIS

To quantify the effect of these differences a series of optical model fits was obtained, starting from six different initial potentials: three where both real and imaginary potentials were of Woods-Saxon form, viz., the 22 MeV ^{6}He +^{208}Pb parameters of Ref. [2] and the ^{6}Li and ^{7}Li global parameters of Ref. [13], and three where the real potentials were calculated using the double-folding procedure [14] while the Woods-Saxon form was retained for the imaginary potentials. Parameter searches were carried out with SFRESCO, the searching version of the FRESCO code [15]. The double-folding potentials were calculated using the code DFPOT [16], with the M3Y effective nucleon-nucleon interaction [17] and the ^{208}Pb matter density of Ref. [18]. The three ^{8}He densities were taken from Refs. [19–21].

All six searches yield identical fits to the data, χ^2/N varying from 3.76 to 3.95 and the total reaction cross section ($\sigma_{\rm R}$) from 1513 to 1530 mb, with a mean value of 1522 mb. The real potentials cross in a radial region defined by $r = 12.75 \pm 0.55$ fm and are split into two families, one much more diffuse than the other. Therefore, as is usual for heavy ion elastic scattering, the real potential is only defined by the data in a relatively narrow radial range in the surface region, of the order of ± 0.5 fm; see, e.g., Satchler [22]. By contrast, the imaginary potentials coincide very closely over a wide radial range, conservatively defined by $r = 15.5 \pm 1.5$ fm. Thus not only is the imaginary potential defined by the data at a larger radius than the real potential—a feature often found in stable heavy ion elastic scattering—it is also well defined over a considerable radial range, which is not usual. In Table I we give

TABLE I. Optical model parameters fitting the 22 MeV ^{8}He and ^{6}He +^{208}Pb elastic scattering data. Radii follow the convention $R_i = r_i \times A_t^{1/3}$ fm and $r_C = 1.3$ fm.

Projectile	V	r_V	a_V	W	r_W	a_W	$\sigma_{\rm R}$ (mb)	χ^2/N
^{8}He	157.1	1.651	0.557	10.5	1.733	1.137	1520	3.76
^{6}He	114.2	1.286	0.632	9.44	1.247	1.865	1459	0.91

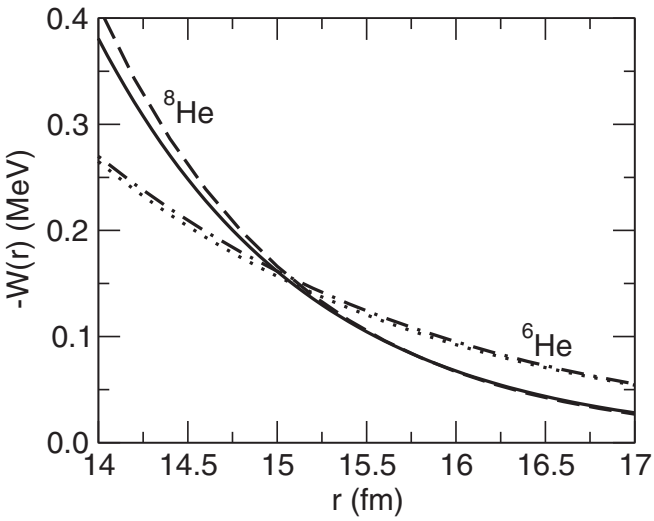

FIG. 3. Solid and dashed curves: imaginary parts of two of the best fit 22 MeV ^{8}He $+^{208}$Pb optical model potentials. Dotted and dot-dashed curves: imaginary parts of two of the best fit 22 MeV ^{6}He $+^{208}$Pb optical model potentials. The other best fit potentials are omitted for the sake of clarity but coincide equally closely over this radial range.

the parameters of the optical model fit to the ^{8}He $+^{208}$Pb data obtained with the global ^{7}Li parameters of Ref. [13] as starting point. The fit to the data with these parameters is plotted in Fig. 2(a) as the solid curve (the fits with the other potentials are indistinguishable). In Fig. 3 we plot the imaginary parts of two of the best fit potentials as a function of radius over the range $14 \leqslant r \leqslant 17$ fm as the solid and dashed lines.

These potentials may be compared with fits to the existing 22 MeV ^{6}He $+^{208}$Pb data. Additional data [3] have become available since the original work [2] and therefore we have combined these two data sets to yield the angular distribution shown in Fig. 2(a). To fit the combined data we adopted a similar procedure to that used for the ^{8}He data, taking the global ^{6}Li and ^{7}Li parameters of Ref. [13] and double folded real (calculated using ^{6}He matter densities from Refs. [20,21,23]) plus Woods-Saxon imaginary potentials as starting points. All five searches give identical fits to the combined data, with χ^2/N values ranging from 0.89 to 0.91 and σ_R from 1456 to 1463 mb, with a mean value of 1459 mb. The real potentials cross in a radial region defined by $r = 10.2 \pm 0.4$ fm while the imaginary potentials coincide over a similar radial range to those for ^{8}He. In Table I we also give the parameters of the optical model fit to the ^{6}He $+^{208}$Pb data obtained with the global ^{7}Li parameters of Ref. [13] as starting point. The fit to the data is plotted in Fig. 2(a) as the dashed curve (the fits with the other potentials are indistinguishable) and in Fig. 3 we plot the imaginary parts of two of the best fit potentials as the dotted and dot-dashed lines.

IV. CONCLUSIONS

Since the data are sensitive to the real potentials at different radii for the two systems, we concentrate on the imaginary potentials where a meaningful point-by-point comparison can be made. However, we note that neither data set requires a large real diffuseness, good fits being possible with values similar to those obtained for stable heavy ion projectiles (see Table I), indicating that the elastic scattering angular distributions are not sensitive to the presence or absence of any long-range real DPP due, for example, to breakup processes, that may be theoretically predicted.

Figure 3 shows that the ^{6}He imaginary potential is more diffuse than the ^{8}He one, although the latter is more absorptive overall, consistent with the larger total reaction cross section for ^{8}He. The less diffuse nature of the ^{8}He imaginary potential points to a reduced importance of breakup compared to ^{6}He, since it has been shown explicitly that Coulomb dipole coupling to the continuum generates a long tail in the imaginary as well as the real potential for the ^{6}He $+^{208}$Pb system; see, e.g.. Ref. [24]. The greater total absorption observed here in the ^{8}He $+^{208}$Pb system compared to ^{6}He $+^{208}$Pb is perfectly consistent with this, since it has been demonstrated by coincidence measurements that the majority of the inclusive α-particle yield (and at near-barrier energies this dominates the total reaction cross section) for ^{6}He interacting with heavy targets is produced by $1n$- and $2n$-stripping reactions (see, e.g., [25–27]), and neutron transfers have also been shown to dominate the absorption in the interaction of ^{8}He with a heavy target [28], while the near-barrier fusion cross sections for ^{6}He and ^{8}He are essentially identical [28]. The optical model potentials therefore point to an increased importance of neutron-stripping transfer reactions for ^{8}He which more than compensates for a reduced breakup cross section. It is important to underline that Fig. 3 shows that there is significant absorption for both isotopes at radii well beyond the conventional strong absorption radius (r_{sa}); the r_{sa}, defined as the radius at which $|S_L| = 0.5$, are 13.4 and 12.2 fm for ^{8}He and ^{6}He, respectively. Figure 2(b) reinforces these conclusions, demonstrating as it does that the absorption in the ^{6}He $+^{208}$Pb system has a considerably longer range than for ^{8}He $+^{208}$Pb.

In summary, we have presented the first complete angular distribution for the elastic scattering of ^{8}He from a heavy target. Due to the quality of the SPIRAL beam and the resolution of the GLORIA detector array, the data are of comparable precision to the best stable beam data. Important differences were observed between these data and those for elastic scattering of ^{6}He from the same target at the same beam energy. These differences were quantified through comparison of optical model potentials fitting the respective data sets and may be explained by the differing properties of the two isotopes. Further work will investigate explicitly the differing influences of neutron-stripping couplings on ^{6}He and ^{8}He elastic scattering from heavy targets, these two isotopes providing an excellent test case for probing these effects.

ACKNOWLEDGMENTS

The authors would like to thank the staff of the GANIL accelerator facility for providing the high quality ^{8}He beam. This work was supported in part by Grant No. FPA2010-22131-C02-01 (FINURA) and Grant No. FPA2013-47327-C2-1-R from the Spanish Ministry of Economy and Competitiveness,

UNAM-PAPIIT IA101616 (Mexico), Grant No. N202 033637 from the Ministry of Science and Higher Education of Poland, and Contract No. EUI2009-04163 (EUROGENESIS) from the European Science Foundation.

[1] N. Keeley, K. W. Kemper, and K. Rusek, Eur. Phys. J. A **50**, 145 (2014).
[2] A. M. Sánchez-Benítez *et al.*, Nucl. Phys. A **803**, 30 (2008).
[3] L. Acosta, A. M. Sanchez-Benitez, M. E. Gomez, I. Martel, F. Perez-Bernal, F. Pizarro, J. Rodriguez-Quintero, K. Rusek, M. A. G. Alvarez, M. V. Andres, J. M. Espino, J. P. Fernandez-Garcia, J. Gomez-Camacho, A. M. Moro, C. Angulo, J. Cabrera, E. Casarejos, P. Demaret, M. J. G. Borge, D. Escrig, O. Tengblad, S. Cherubini, P. Figuera, M. Gulino, M. Freer, C. Metelko, V. Ziman, R. Raabe, I. Mukha, D. Smirnov, O. R. Kakuee, and J. Rahighi, Phys. Rev. C **84**, 044604 (2011).
[4] V. Lapoux and N. Alamanos, Eur. Phys. J. A **51**, 91 (2015).
[5] N. Keeley, N. Alamanos, K. W. Kemper, and K. Rusek, Prog. Part. Nucl. Phys. **63**, 396 (2009).
[6] G. Marquínez-Durán *et al.*, Acta Phys. Pol. B **43**, 239 (2012).
[7] G. Marquínez-Durán *et al.*, Acta Phys. Pol. B **44**, 467 (2013).
[8] G. Marquínez-Durán *et al.*, in *La Rábida 2012: International Scientific Meeting on Nuclear Physics*, September 2012, La Rábida, Spain, edited by J. A. Caballero Carretero, C. E. Alonso Alonso, M. V. Andrés Martín, J. E. Garcia Ramos, and F. Pérez Bernal, AIP Conf. Proc. No. 1541 (AIP, New York, 2013), p. 175.
[9] G. Marquínez-Durán *et al.*, EPJ Web Conf. **66**, 03058 (2014).
[10] G. Marquínez-Durán *et al.*, Nucl. Instrum. Methods Phys. Res. A **755**, 69 (2014).
[11] G. Marquínez-Durán *et al.*, Acta Phys. Pol. B **47**, 841 (2016).
[12] The NPTool package, https://github.com/adrien-matta/nptool.
[13] J. Cook, Nucl. Phys. A **388**, 153 (1982).
[14] G. R. Satchler and W. G. Love, Phys. Rep. **55**, 183 (1979).
[15] I. J. Thompson, Comput. Phys. Rep. **7**, 167 (1988).
[16] J. Cook, Comput. Phys. Commum. **25**, 125 (1982).
[17] G. Bertsch, J. Borysowicz, H. McManus, and W. G. Love, Nucl. Phys. A **284**, 399 (1977).
[18] G. R. Satchler, Nucl. Phys. A **579**, 241 (1994)
[19] P. Navrátil and B. R. Barrett, Phys. Rev. C **57**, 3119 (1998).
[20] I. Tanihata, D. Hirata, T. Kobayashi, S. Shimoura, K. Sugimoto, and H. Toki, Phys. Lett. B **289**, 261 (1992).
[21] A. Bhagwat, Y. K. Gambhir, and S. H. Patil, Eur. Phys. J. A **8**, 511 (2000).
[22] G. R. Satchler, *Direct Nuclear Reactions* (Clarendon, Oxford, 1983), p. 500.
[23] J. S. Al-Khalili, J. A. Tostevin, and I. J. Thompson, Phys. Rev. C **54**, 1843 (1996).
[24] R. S. Mackintosh and N. Keeley, Phys. Rev. C **79**, 014611 (2009).
[25] J. P. Bychowski *et al.*, Phys. Lett. B **596**, 26 (2004).
[26] P. A. DeYoung, P. J. Mears, J. J. Kolata, E. F. Aguilera, F. D. Becchetti, Y. Chen, M. Cloughesy, H. Griffin, C. Guess, J. D. Hinnefeld, H. Jiang, S. R. Jones, U. Khadka, D. Lizcano, E. Martinez-Quiroz, M. Ojaniega, G. F. Peaslee, A. Pena, J. Rieth, S. Van Den Driessche, and J. A. Zimmerman, Phys. Rev. C **71**, 051601 (2005).
[27] J. J. Kolata, H. Amro, F. D. Becchetti, J. A. Brown, P. A. DeYoung, M. Hencheck, J. D. Hinnefeld, G. F. Peaslee, A. L. Fritsch, C. Hall, U. Khadka, P. J. Mears, P. ORourke, D. Padilla, J. Rieth, T. Spencer, and T. Williams, Phys. Rev. C **75**, 031302 (2007).
[28] A. Lemasson, A. Shrivastava, A. Navin, M. Rejmund, N. Keeley, V. Zelevinsky, S. Bhattacharyya, A. Chatterjee, G. deFrance, B. Jacquot, V. Nanal, R. G. Pillay, R. Raabe, and C. Schmitt, Phys. Rev. Lett. **103**, 232701 (2009).